Journal of Structural Biology **136,** 20–29 (2001)
doi:10.1006/jsbi.2001.4422, available online at http://www.idealibrary.com on IDEAL®

Correlation of Topographic Surface and Volume Data from Three-Dimensional Electron Microscopy

Eva Dimmeler, Roberto Marabini,† Peter Tittmann, and Heinz Gross[1]

Swiss Federal Institute of Technology (ETH Zürich), Institute of Applied Physics, CH-8093 Zürich, Switzerland; and †Graduate School and University Center, City University of New York, New York, New York

Received September 13, 2000, and in revised form November 13, 2001

Three-dimensional (3D) reconstructions from tilt series in an electron microscope show in general an anisotropic resolution due to an instrumentally limited tilt angle. As a consequence, the information in the *z* direction is blurred, thus making it difficult to detect the boundary of the reconstructed structures. In contrast, high-resolution topography data from microscopic surface techniques provide exactly complementary information. The combination of topographic surface and volume data leads to a better understanding of the 3D structure. The new correlation procedure presented determines both the height scaling of the topographic surface and the relative position of surface and volume data, thus allowing information to be combined. Experimental data for crystalline T4 bacteriophage polyheads were used to test the new method. Three-dimensional volume data were reconstructed from a negatively stained tilt series. Topographic data for both surfaces were obtained by surface relief reconstruction of electron micrographs of freeze-dried and unidirectionally metal-shadowed polyheads. The combined visualization of volume data with the scaled and aligned surface data shows that the correlation technique yields meaningful results. The reported correlation method may be applied to surface data obtained by any microscopic technique yielding topographic data. © 2001 Elsevier Science (USA)

Key Words: **alignment; correlation; three-dimensional reconstruction; registration; surface; T4 polyhead; transmission electron microscopy; volume.**

INTRODUCTION

Three-dimensional structure determination in the transmission electron microscope (TEM) is based on a combination of many two-dimensional (2D) views of the same object, each seen from a different viewing angle. In the case of helices or many identical single particles oriented randomly on the TEM grid the whole 3D space is directly accessible (Frank, 1996). For all other samples that adopt a preferred orientation on the support film the different views are realized by tilting the specimen. Owing to the restricted tilting range in a TEM information is lacking in a cone or wedge perpendicular to the tilt axis. This results in a blurring along the *z* direction of the reconstructed structure and, therefore, in a blurred surface reproduction. The boundary of the reconstructed structures is not clearly defined (Fig. 1). This information gap could be filled if complementary surface data were available. There are different techniques to determine the surface topography of macromolecular structures, e.g., scanning electron microscopy, atomic force microscopy, and unidirectional metal shadowing in the TEM.

The surface reconstruction of images of freeze-dried and subsequently heavy metal-shadowed samples is a well-established technique that has been continuously improved in our laboratory (Gross, 1987). Today, it is possible to resolve surface details of 2D crystalline objects at a spatial resolution of 15–8 Å laterally and <5 Å vertically, depending on the quality of the crystals (Walz *et al.*, 1996). The progress is based mainly on the in-house developed MIDILAB (Gross *et al.*, 1990), allowing the freeze-dried and shadowed specimens to be transferred into the cryo-TEM under high vacuum and cryo conditions. Consequently, a stabilizing carbon coat obscuring fine-structural details is no longer necessary.

The problem of combining data from different techniques to give 3D information is well known in medicine (intermodality image registration). Several algorithms are used to correlate volume with volume data, surface with surface data, or mixed (West *et al.*, 1999). We use a completely different

[1] To whom correspondence should be addressed. E-mail: gross@iap.phys.ethz.ch.

1047-8477/01 $35.00

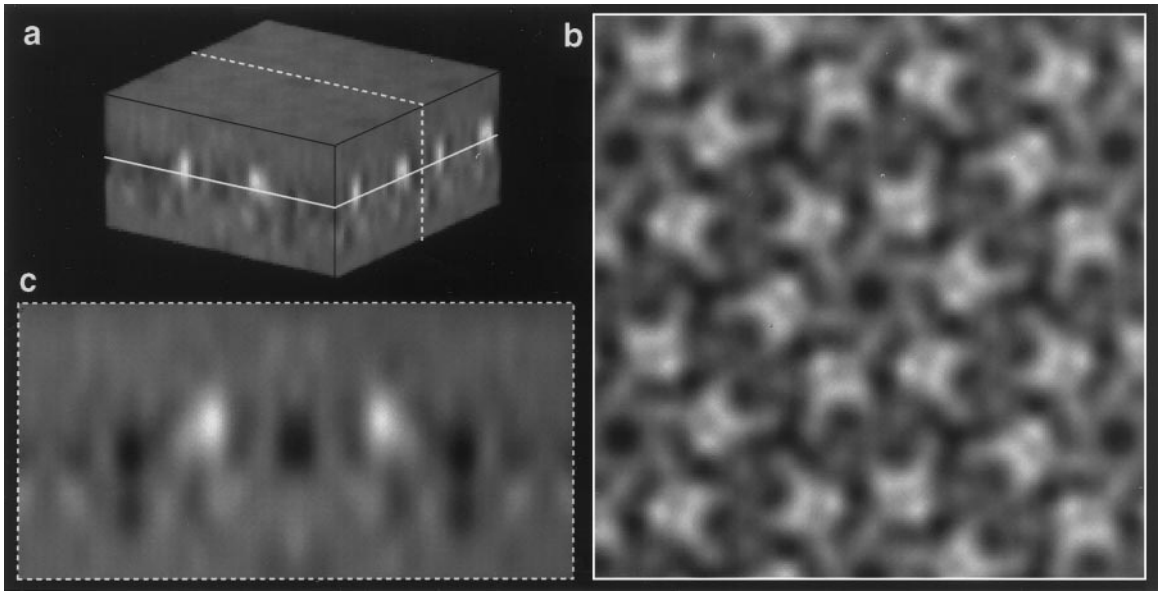

FIG. 1. Volume reconstruction of a negatively stained polyhead from the projections of one tilt series. (a) Volume-rendered cube. The white lines indicate the 2D sections (solid line: *x–y* section, dotted line: *x–z* section). (b) The *x–y* section shows clearly defined structures with a lateral resolution of 12 Å. (c) In axial direction (*x–z* section) the reconstructed data are strongly blurred owing to the restricted tilt range, thus preventing the definition of the boundary of the reconstructed structures.

solution to correlate surface with volume data. First, in contrast to typical medical volume data (e.g., magnetic resonance imaging (MRI) or computer tomography (CT) scans), 3D reconstructed volume data from TEM have a strong anisotropic resolution. Second, in the medical context surface data represent the closed boundary of a 3D object. In contrast, all of the above-mentioned microscopic surface methods detect the topography of an object and yield information only for that part of the object, which is exposed to the scanning tip or to the metal coat. Therefore, many restrictions are given by the experimental setup which reduces the number of degrees of freedom for the alignment problem. This facilitates the combination of volume data from a TEM and topographic surface data.

Combination of topographic surface and volume data could be performed in three different ways: (i) by visual arrangement of surface with volume data in 3D space, (ii) by using an algorithmic correlation of surface data with the independently reconstructed volume data from 2D projections, and (iii) by integrating surface information directly in the 3D reconstruction procedure. Point iii is currently being addressed by incorporating the surface reliefs as constraints in the algebraic reconstruction technique (ART) algorithm (Marabini *et al.*, 1998; Herman *et al.*, 2000).

Here we concentrate on the first two approaches, the visual and algorithmic combination of surface and volume data of a 2D crystalline object, the polyheads of bacteriophage T4 (type III). Surface data were obtained by the unidirectionally metal shadowing technique in the TEM (Fig. 2). Volume reconstruction from a negatively stained tilt series was performed by processing and combining images with angles between −60° and +60°.

In this article we first present the basic idea of the algorithmic correlation of surface with volume data via projections and correlation functions. Then the results of applying the new method to both the outer and inner surfaces of polyhead tubes are shown, and the limits of visual and algorithmic alignment are discussed.

MATERIALS AND METHODS

1. Polyhead Preparation

The bacteriophage T4 type III polyhead is an aberrant mutant of the T4 phage and is composed of capsomeres of gene product 23 (gp23), arranged on a near-hexagonal lattice which is folded into a cylinder. The tubes present essentially the same hexagonal capsid pattern as on the native bacteriophage head. When adsorbed to a support film, the spread-flattened tubes expose a quasi-2D crystal with a quasi-*p*6 symmetry and a lattice constant of 13 nm (Steven *et al.*, 1976). A capsomere consists of six protomeres with a "pore-like" structure on the sixfold axes. The bacteriophage T4 type III polyheads were prepared as described by Steven *et al.* (1976) and provided by U. Aebi (Basel).

Volume data were acquired after negative staining with 2% uranyl acetate. Surface data were obtained after freeze-drying and unidirectionally shadowing at −80°C with Ta/W at an elevation angle of 45°. Because of its tubular structure a polyhead has two surfaces, an outer surface and a hidden inner surface. The only access to the topography of the inner surface is given by

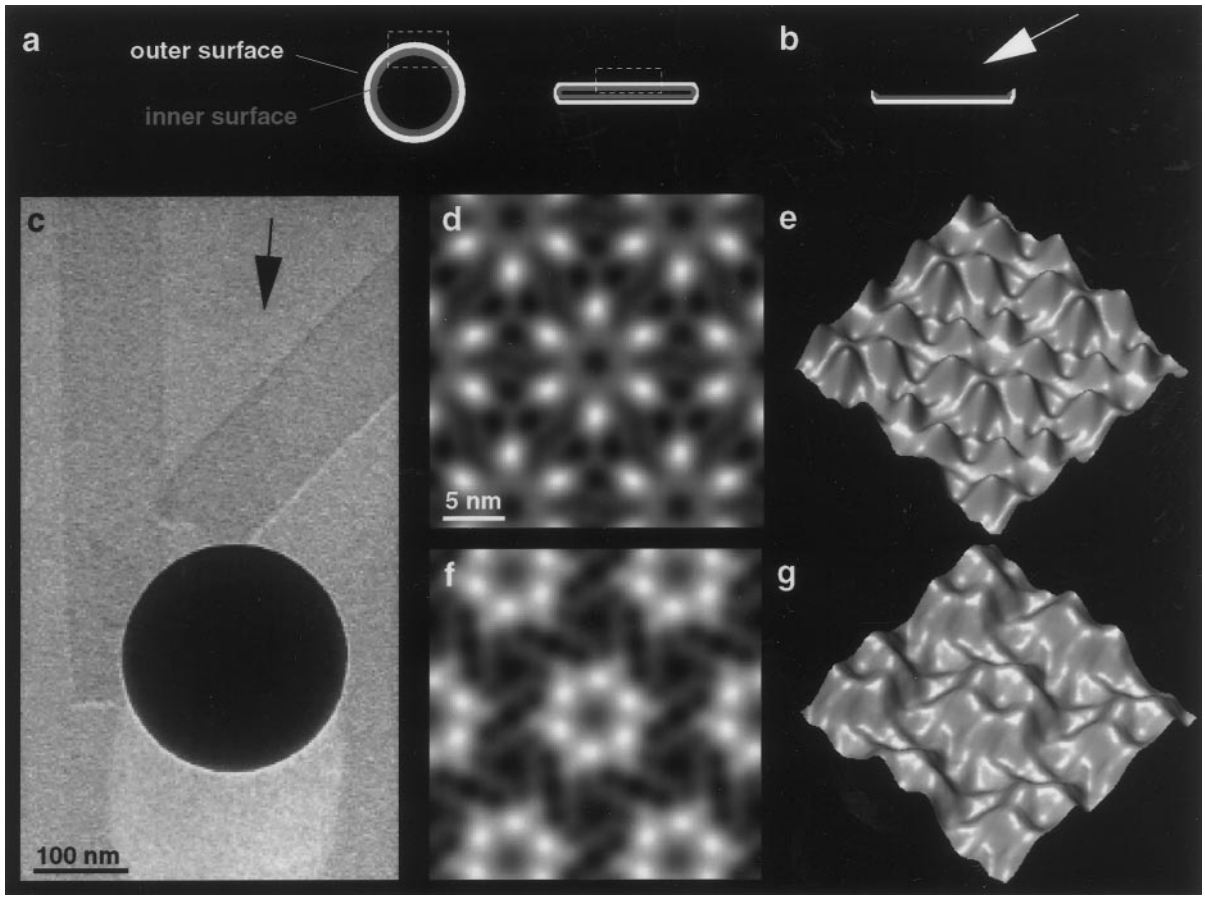

FIG. 2. (a) Cross section through a polyhead cylinder showing the outer and inner surfaces. During preparation the cylinders are flattened (right). The dotted square indicates the 2D crystalline area, which is reconstructed from the tilt series and shown in Fig. 1 as volume data. (b) Dissected polyhead tube, allowing metal shadowing (indicated by the arrow) of the inner surface. (c) Electron micrograph of two freeze-dried and unidirectionally metal shadowed polyhead cylinders. The shadowing direction (black arrow) can be concluded from the shadow caused by a coprepared latex sphere (black circle). (d) Top view and (e) 3D view of the outer surface of the polyhead after relief reconstruction. (f) Top view and (g) 3D view of the reconstructed inner surface. For a better visibility of the surface features the height of the 3D views is overscaled.

finding dissected tubes, which then allows shadowing of the inner surface (Fig. 2b).

2. Processing of Surface Data

Images were taken on film (Agfa Scientia) under low-dose conditions (electron dose $<10e^{-}/Å^{2}$) at magnifications of 45 000× (outer surface) and and 40 000× (inner surface), respectively. Scanning of the negatives yielded pixel sizes of 2.1 Å for the outer surface and 2.7 Å for the inner surface. The crystalline areas were correlation averaged to improve the signal-to-noise ratio, and the resolution (Fourier ring correlation criterion, Saxton and Baumeister, 1982) was determined to be 13 Å in the *x–y* direction for both surfaces. The amount of metal deposited provides a direct measure of the gradient of the surface and was used to calculate the surface topography from the averaged images (Fuchs *et al.*, 1995). The sixfold symmetry of the polyhead structure allowed reconstruction of complete surface data from a single micrograph. The *x–y* calibration was given by the pixel size. Basically, the *z* calibration of the surface could be calculated from the gradient. But long experience has shown that this value is only a rough estimate, and higher accuracy may be obtained by other experimental techniques.

3. Processing of Volume Data

A single tilt series of 17 images were acquired at room temperature under low-dose conditions (total accumulated dose: $85e^{-}/Å^{2}$) in a Philips TEM CM12 which was operated at an acceleration voltage of 100 kV. Images were recorded with a Gatan (694) slow-scan CCD camera (24-μm pixels) at a magnification of 56 500×, corresponding to 4.1-Å pixel size at specimen level. The tilted images covered a tilt range from +60° to −60°, and the angular steps followed a scheme proposed a by Saxton and Baumeister (1984). Square areas of 1024 × 1024 pixels of the selected views were processed using a combination of software packages to take advantage of their different capabilities. Most of the software belonged to the MRC suite (Crowther *et al.*, 1996). Lattice separation and refinement were carried out using the X-Window-based graphical environment SPECTRA (Schmid *et al.*, 1993). Lattice distortion correction was performed by the methods described in Henderson *et al.* (1986). In most cases one

cycle of lattice unbending was sufficient. The resolution obtained in the final map was calculated to be 12 Å in the *x–y* plane and 18 Å in the *z* direction.

4. Principle of Alignment of Surface and Volume Data

For specimens whose structure is determined by a tilt series in a TEM the alignment problem is straightforward, because the orientation of the surface relative to the volume is given by the experimental setup. All known surface techniques detect a topography (Figs. 2e and 2g) that is oriented parallel to the *x–y* plane in the TEM (indicated by a solid line in Fig. 1a). So the problem has only one rotational and three translational degrees of freedom. Thus, the alignment can be divided into a lateral part (*x–y* direction) and an axial part (*z* direction).

a. Lateral alignment. Surface data are represented by a 2D image top view (Fig. 3b), with gray values encoding the height (*z* value) of the surface. First the surface top view is scaled relative to the volume in the *x–y* direction; i.e., the pixel size of the surface top view is adjusted to the *x–y* pixel size of the volume data. Then the surface top view is both rotationally and translationally aligned relative to selected *x–y* layers of the reconstructed volume using 2D cross-correlation functions (Frank, 1996).

b. Axial alignment. For the axial alignment the volume is assumed to be completely filled with material of constant density (Fig. 3). If exactly that part of the volume that corresponds to the surface is projected in the *z* direction (calculation of the line integral in the *z* direction by adding up all volume elements), the resulting projection (Fig. 3d) is exactly the same as the surface top view (Fig. 3b). Finding the axial alignment entails systematically projecting different parts of the volume and subsequently comparing the projections with the surface top view. The similarity of the projections with the surface top view is measured by the cross-correlation coefficient. The absolute maximum of all cross-correlation coefficients yields the position of the surface relative to the volume, as well as the *z* calibration of surface data since the *z* calibration of the volume data is defined by the voxel size.

5. Alignment of Surface and Volume Data of Tubular T4 Polyheads

When two surfaces are correlated with a volume, both their orientation and handedness have to be carefully considered. The experimental outer surface of a polyhead corresponded directly to that boundary of the molecule in the 3D volume, for which "by definition" the surface vector pointed in the positive *z* direction. To calculate the correlation of the inner surface of the polyhead the experimental 2D surface top view had to be flipped, which means that the surface vector pointed in the negative *z* direction.

Lateral scaling of the reconstructed surfaces was done by adjusting the lattice vectors with that of the 3D volume reconstruction (resampling to a pixel size of 2 Å). No rotational alignment was necessary because surface and volume reconstructions were already oriented with one hexagonal lattice vector horizontally. Lateral translational alignment was performed by calculating the cross-correlation function between the surfaces and selected *x–y* layers of the volume.

For axial alignment, the output from the 3D reconstruction was cropped between a varying bottom and a varying top *x–y* layer before calculation of the projection in the *z* direction. The layer that was farther from the center of the volume was called the top layer, regardless of its actual position in the 3D stack. The top and bottom layers of the projected region, which fits best the surface top view, then correspond directly to the highest and deepest points of the surface, respectively. The projection of the cropped volume part was calculated for each *x–y* position by the addition of all gray values in the *z* direction and subsequent division by the number of projected layers. Such projections were calculated for all possible volume parts by systematically varying both the top and bottom layers defining the cropped region.

To avoid high frequencies in Fourier space during calculation of the cross-correlation function, a hexagon of three unit cells was circularly masked with a Gaussian border (standard deviation 1/24th of the lattice vector) and padded with zero (Frank, 1996) for both the surface top view and the projected region. To decide which projected region had the strongest similarity with the surface top view, normalized cross-correlation coefficients at the origin of the cross-correlation map were compared. Normalization was done by dividing the resulting cross-correlation coefficient by the square root of the product of the autocorrelation coefficients of both 2D images. Comparing the coefficients for a fixed top layer and varying bottom layers, the maximum yields the *z* calibration of the surface for that specific top layer, since the *z* calibration of the volume and therefore the distance between top and found bottom layers is known. Comparison of the correlation maxima for different top layers gives both the correct *z* calibration and the correct axial location of the surface in the volume. The software for the algorithmic combination of 3D volume and surface data was written in-house. The 3D visualization software was developed in collaboration with Bitplane AG, Zürich, Switzerland.

RESULTS

Lateral alignment by calculating the cross-correlation map of the surfaces (Fig. 2) with single *x–y* layers of the reconstructed volume (Fig. 1) was ambiguous. Depending on the chosen *x–y* layer the resulting lateral shift vectors differed by 2 pixels. To overcome this ambiguity the whole axial alignment (Section 4b) was performed several times, each time the surface was shifted by one or two pixels in the *x* or *y* direction or both. The relative result of the axial alignment did not change; i.e., the relation of the cross-correlation coefficients did not change, but the absolute values varied by a multiplicative factor. The maximum indicated the best lateral and axial alignment which was confirmed by visual inspection.

The axial alignment of the outer surface showed clear maxima (Fig. 4a) in the plot of cross-correlation coefficients, describing the similarity of cropped regions with a fixed top layer and varying bottom layers. Three different types of curves were observed. Curves with one maximum in the center indicate that the surface is either outside of the volume; e.g., the chosen top layer is still too far away from the center of the molecule (Fig. 5a) or at precisely the correct location in the volume (Fig. 5b). Curves with two maxima show that the surface is inside the volume (Fig. 5c). The third type of curve with a maximum at the end means that the surface top view is most similar to a single *x–y* layer, the bottom layer, in the volume, rather than to a projection. This is the case if the top layer is chosen too far inside the volume. The maximum cross-correlation coefficient for the outer surface of the polyhead (Fig. 4b) was found in a curve showing one centered maximum, clearly indicating a good match of surface

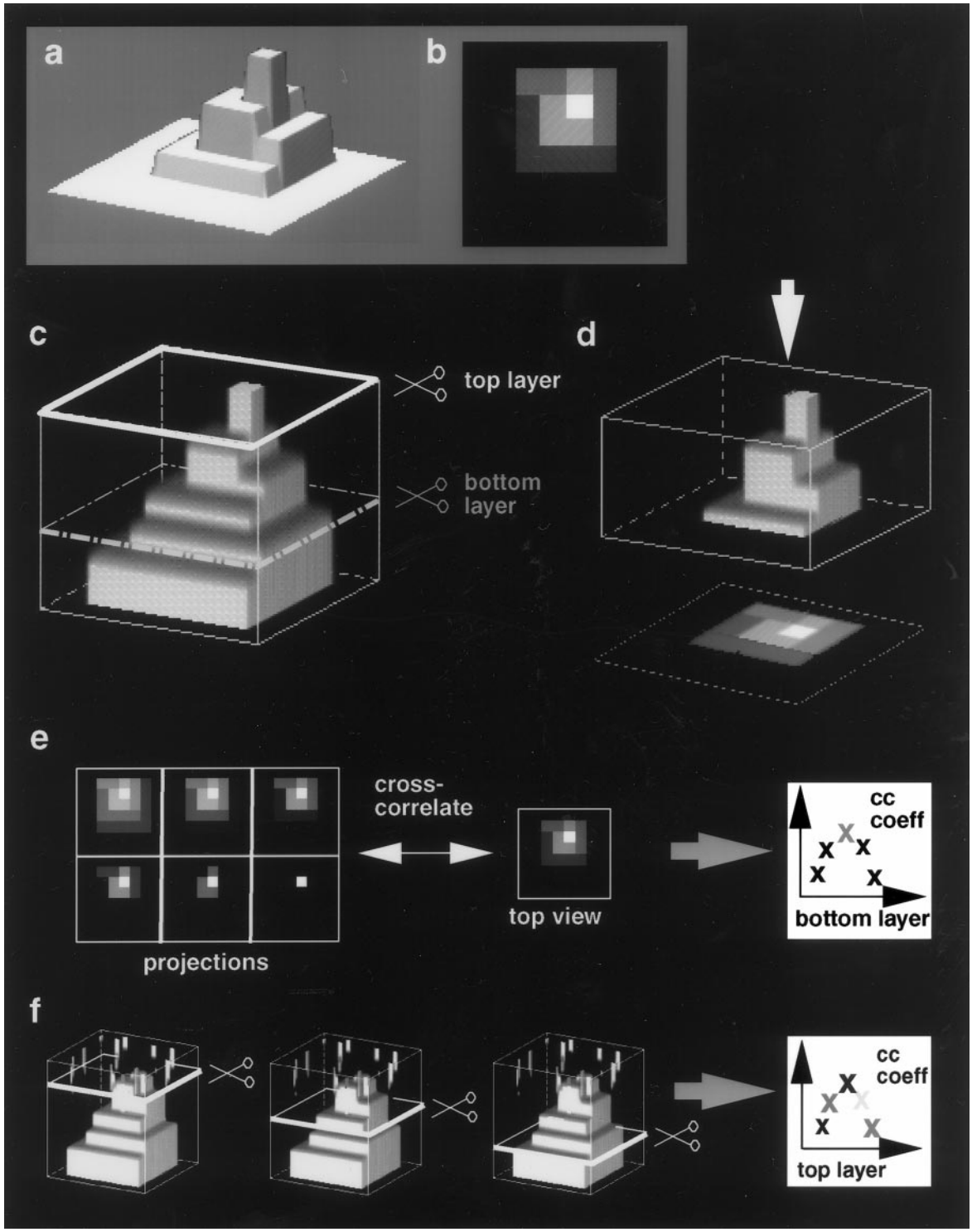

FIG. 3. Surface and volume data of a model object. The surface (a) fits exactly to the upper part of the volume (c). (a) Three-dimensional view and (b) top view of the surface. (c) Volume data are visualized by ray tracing. The dotted line indicates the height corresponding to the deepest point of the surface. (d) Upper part of the volume cut between top and bottom layers indicated in (c) and the 2D projection image, which results from summation over all volume elements in the *z* direction as indicated by the arrow. This projection image is identical to the surface top view shown in (b). (e) and (f) explain the correlation-based search for the top and bottom layers defining a cropped region of the volume, for which the projection is most similar to the surface top view. (e) In the first step the volume is cropped between a certain top layer and varying bottom layers, and the projections of the cropped regions (left) are cross-correlated with the surface top view (center). The resulting correlation coefficients are plotted against the bottom layer (right), the maximum thus

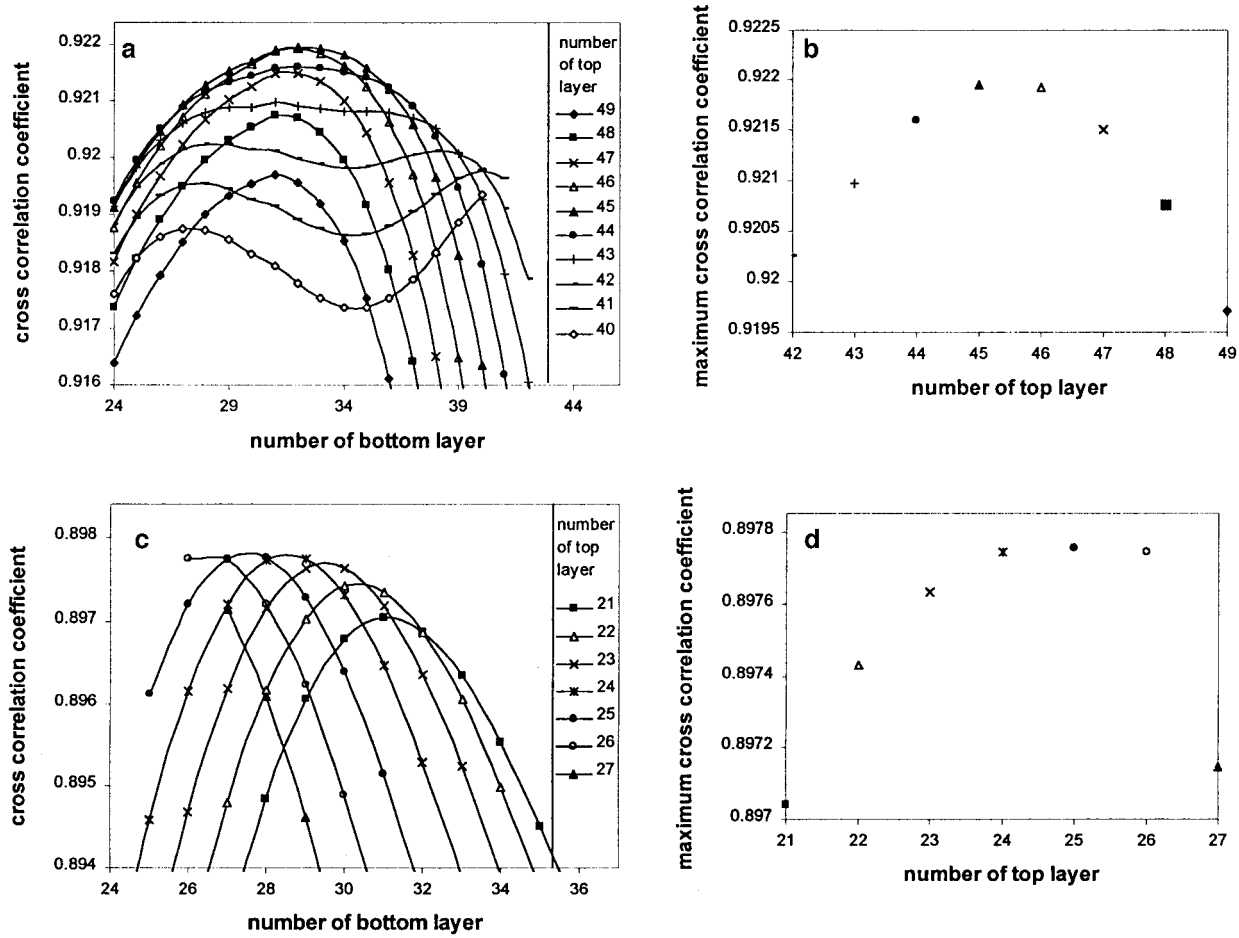

FIG. 4. Cross-correlation results for the outer (a, b) and inner (c, d) surfaces of the polyhead. (a) Each curve shows normalized coefficients for the cross-correlation between the top view of the outer surface and the projection image of part of the volume, which was cut at a certain top layer (cf. plot in Fig. 3e). Each point of the curve stands for a volume part, which was cut at a different bottom layer. The plot shows several curves covering all combinations of top and bottom layers. The maximum of a single curve yields the corresponding *z* calibration of the surface by simply counting the enclosed *x*–*y* layers of the volume and taking into account the known *z* calibration of the volume. (b) The maxima of the curves in (a) are plotted against the top layer to obtain the absolute maximum cross-correlation coefficient (cf. plot in Fig. 3f). The maximum is clearly defined and yields an outer surface with a thickness variation of 28 Å and the fixation of the deepest point of the surface in the volume at a height of 64 Å. which is visualized in Fig. 5b. (c) Cross-correlation coefficients for projected volume parts of the inner surface. (d) Maxima of the correlation curves in (c). The absolute maximum cross-correlation coefficient yields an inner surface with a thickness variation of 8 Å, the highest point fixed at an height of 54 Å in the volume.

with volume. The resulting *z* calibration assigns a thickness variation of 28 Å for the outer surface of the polyhead, measured from the deepest to the highest point of the surface (Fig. 6).

The axial alignment of the inner surface of the polyhead resulted in two types of curves, one with a maximum at the center and one with a maximum at the end (Fig. 4c). The maximum cross-correlation coefficient was found in a curve with a centered maximum (Fig. 4d). The second highest cross-correlation maximum appeared at the end of a correlation curve. The corresponding top-to-bottom layer distance yielded a thickness variation of 8 Å for the inner surface (Fig. 6).

Knowledge of the *z* calibration and the location of both polyhead surfaces relative to the reconstructed

indicating the "best" bottom layer for that specific top layer. (f) To obtain the correct *z* position and *z* calibration of the surface, the whole procedure described in (e) is repeated for volume parts cropped at different top layers. All maxima of the correlation curves in (e) are plotted against the top layer. The absolute maximum yields a top and bottom layer limiting that region of the volume, which resembles best the experimental surface.

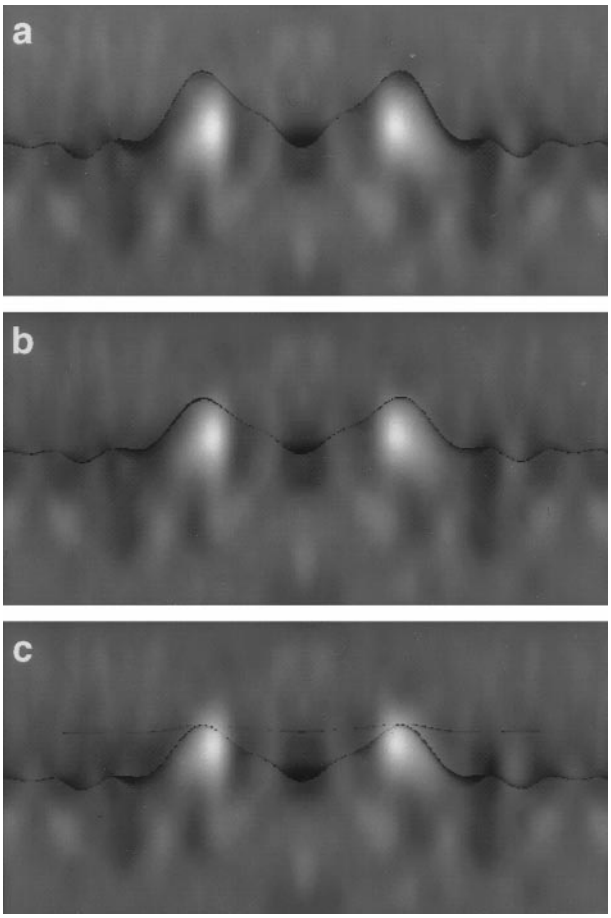

FIG. 5. Simultaneous visualization of a semitransparent *x*–*z* view of the volume (same view as in Fig. 1c) and the outer surface indicated by a black curved line. As the surface is represented as a 3D view cut in a special *x*–*z* plane, parts of the surface behind that plane can be seen where the volume has low density. (a–c) Different *z* scaling and *z* alignment of the outer surface relative to the volume, thereby elucidating some correlation maxima in Fig. 4b. (a) Maximum cross-correlation coefficient for a chosen top layer No. 49 yields a surface thickness of 38 Å, which is given by the maximum of the curve with filled rhombs in Fig. 4a. (b) The absolute cross correlation maximum appears for top layer No. 45 and reveals a surface thickness of 28 Å (curve with filled triangles in Figs. 4a and 4b). This calibration shows also visually the best fit of surface to volume data, which can be verified in other sections (data not shown). (c) This *x*–*z* section visualizes the correlation result for top layer No. 41: The curve (with flat horizontal stripes in Fig. 4a) of cross-correlation coefficients has two local maxima. Both resulting outer surfaces with thicknesses of 28 Å (thicker line) and 4 Å (very weak line), respectively, are clearly inside the volume.

3D volume was then used to calculate an average protein mass, filling the space between the surfaces. Assuming a protein density of 1.3 g/cm^3 the surfaces include a mass of 263.4 kDa per unit cell. This corresponds to 90.1% of the mass calculated from the known amino acid sequence (Parker *et al.*, 1984).

DISCUSSION

Application of the new method for correlating surface and volume data to our experimental test object, the bacteriophage T4 polyhead, yielded different results for the two surfaces, but the general behavior of the correlation method was the same. An indication of the validity of the correlation method is the shape change observed in the correlation curves as the surfaces are brought successively closer to the center of the molecule (Figs. 4a and 4c). When the surface is still outside of the volume, the curve shows a single maximum at the center, which increases as the top layer position approaches the best fit of surface to volume. Once the surface has entered the volume, correlation curves exhibit either two maxima or one maximum at the end. Even if the surface is shifted in lateral direction by 1 or 2 pixels, the results remain the same except for a global decrease in the cross-correlation coefficients, thus indicating stable correlation.

In the case of the outer polyhead surface (Figs. 2d and 2e) the correlation results clearly indicate that there is one outstanding position and calibration of the surface fitting to the volume data. All correlation curves show a distinct maximum, and the absolute maximum is visibly higher than the other maxima. The simultaneous visualization of volume and the outer surface confirms that the absolute correlation maximum indeed describes the best fit of volume and surface (Fig. 7). The resulting thickness variation of the outer surface of 28 Å seems reasonable according to shadowing length measurements.

The results are ambiguous for the inner polyhead surface (Figs. 2f and 2g). The maximum cross-corre-

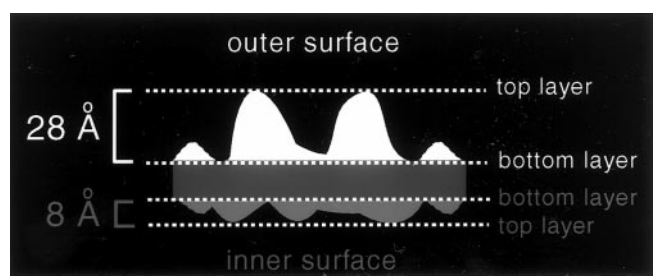

FIG. 6. A schematic *x*–*z* section through the volume data represents the results of the alignment. The maximum correlation for one surface yields a bottom and a top layer, referring to the volume data. The surface is spread between these two layers. With the known *z* calibration of the volume data, which was reconstructed from a tilt series, both the thickness variation and the relative position of the surfaces were determined. The outer surface shows a thickness variation of 28 Å, and the inner surface a thickness variation of 8 Å. The distance between both bottom layers was determined to be 10 Å. As bottom layer always that layer is defined that is nearer to the center of the volume. The drawn detail is indicated in Fig. 2a by a dotted rectangle.

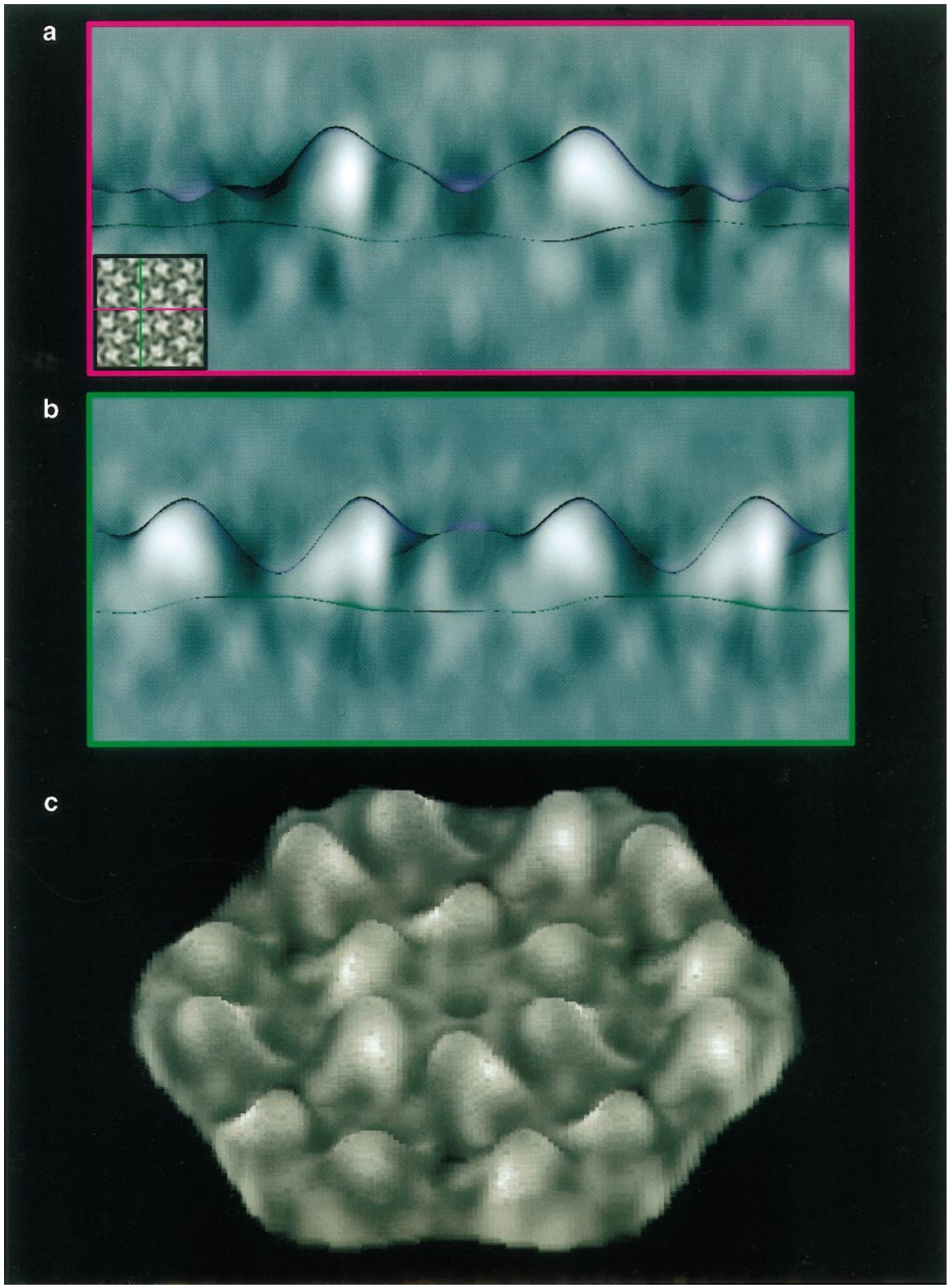

FIG. 7. The results of the best correlation of both surfaces of a polyhead are shown. (a, b) The large images represent an *x*–*z* view and a *y*–*z* view of the volume, with the outer surface colored in purple and the inner surface colored in green. The colored lines in the inset showing the *x*–*y* central layer of the volume indicate the *x*–*z* and *y*–*z* sections respectively. (c) A volume-rendered representation of the polyhead 3D reconstruction after removal of all density outside the aligned surfaces. The parameters for the rendering are the same as in Fig. 1a, thus showing clearly the benefits of combining surface data with incomplete volume data.

lation coefficient is located in the center of a curve, resulting in a surface thickness of 8 Å. But the second highest cross-correlation maximum is found at the end of a correlation curve, thus revealing the second best fit of the surface with a single *x–y* layer of the volume. This implies that the inner surface does not resemble the structural details of the volume very well, which is confirmed by the simultaneous visualization of the inner surface and the volume (Fig. 7).

There are several explanations for the different similarity of both polyhead surfaces with the volume data. Negative staining, which is used for preparation of the tilt series data, imposes restrictions on the validity of the volume data. First, negative staining can cause flattening of surface features due to surface tension forces acting at the air–liquid interface during drying. But as long as mainly the height of surface structures is reduced and no strong structural changes take place, this effect is compensated in the correlation method by the axial scaling of the surface data. By comparing 3D reconstructions of 2D crystalline structures prepared with the frozen hydrated and the negative staining techniques it was shown that at intermediate-resolution (20–15 Å) negative staining can faithfully reproduce the overall structure and size (Hoenger and Aebi, 1996).

Another point is that uranyl acetate does not stain the structure homogeneously, but rather forms an envelope around the examined structure. This can be critical as the correlation technique is based on the assumption that the volume data have homogeneous density inside. However, examination of the polyhead volume data (e.g., Fig. 1c or 7) gives the impression that the stain is penetrating the structure to such an extent that at least the outer surface is widely homogeneously stained. Indeed, for the outer side the volume and the topographic surface data fit together very well.

The inner surface of the polyhead has different preparation conditions, as the former polyhead cylinders flatten during adsorption, resulting in two crystalline layers with the inner surfaces located inside (Fig. 2a). Thus, the heavy metal stain has no direct access. Due to incomplete staining the volume data may not show the correct structural details for the part of the inner surface. Additionally, structural alterations may be caused by a possible interaction of the touching inner surfaces of the two layers.

Both staining and flattening artifacts could be avoided by applying cryo-electron microscopy to an unstained specimen embedded in vitrified ice. Untilted projection data from frozen hydrated polyheads exist (Lepault, 1985). However, a successful 3D reconstruction has not yet been reported.

In contrast to the volume data, the topographic reconstructions of both surfaces of the polyhead should reveal the same high quality due to the identical exposition of the surfaces during the whole preparation process. Thus, the surface data were used to build a 3D model according to Fig. 6. As the calculated mass included between the surfaces corresponds to 90% of the known amino acid mass (Parker *et al.*, 1984), it can be concluded that the resulting position of the inner surface is not far from the true position, assuming that the outer surface is correctly scaled and aligned. Therefore, it seems to be reasonable to build a 3D model by putting the surfaces into the volume according to the correlation results and setting all density outside the surfaces to zero (Fig. 7c).

It should be noted that the alignment method is based on gray values of the real volume, not on a binary version (isosurface) where a threshold has to be set in advance. Thus, the full information given by the 3D reconstruction is used. This may be one reason why the method works despite the fact that the assumption of a constant density within the volume is not strictly fulfilled.

Whether the correlation of surface data with volume data showing artifacts owing to missing information is justified can be discussed. Strictly considered in a mathematical sense, only direct inclusion of surface data in the 3D reconstruction procedure, e.g., with ART, yields correct structural data. But in most cases the inherent inexactness of the a posteriori combination of nonperfect data may be much smaller than the experimental variability of the investigated object itself. The resulting 3D model shows many more details than the pure volume data. So structural determination benefits from this new method.

The novel alignment method is not bound to a special technique for structure determination; in particular it is not limited to crystalline samples. Basically, all blurred volume data can be used, where the boundary of the object is not clearly defined. The topographic surface data could also originate from tip microscopies. The necessary condition for the algorithmic correlation is that the investigated object does not show large hollow regions below the topographic surface.

We thank U. Aebi (Maurice Müller Institute, Basel) for providing the polyheads. We also thank J. M. Carazo, C. O. Sanchez Sorzano (both Centro Nacional de Biotechnologia, Madrid), and G. T. Herman (Graduate School and University Center, City University of New York) for many fruitful discussions, and S. Müller (Maurice Müller Institute, Basel) for critically reading the manuscript. E. Dimmeler was supported by the Swiss Commission of Technology and Innovation (Grant 3272.1). R. Marabini was partially supported by a fellowship from the Spanish Ministery of Education and Science and NIH Grant HL28438.

REFERENCES

Crowther, R. A., Henderson, R., and Smith, J. M. (1996) MRC image processing programs. *J. Struct. Biol.* **116,** 9–16.

Frank, J. (1996) Three-Dimensional Electron Microscopy of Macromolecular Assemblies, Academic Press, San Diego.

Fuchs, K. H., Tittmann, P., Krusche, K., and Gross, H. (1995) Reconstruction and representation of surface data from two-dimensional crystalline, biological macromolecules. *Bioimaging* **3,** 12–24.

Gross, H. (1987) High resolution metal replication of freeze-dried specimens, *in* Steinbrecht, R. A., and Zierold, K. (Ed), Cryotechniques in Biological Electron Microscopy, pp. 205–215, Springer-Verlag, Berlin.

Gross, H., Krusche, K., and Tittmann, P. (1990) Recent progress in high-resolution shadowing for biological transmission electron micrsocopy *in* Proceedings XIIth International Congress on Electron Microscopy, Seattle, pp. 510–511, San Francisco Press, San Francisco.

Henderson, R., Baldwin, J. M., Downing, K. H., Lepault, J., and Zemlin, F. (1986) Structure of purple membrane from *Halobacterium halobium*: Recording, measurement and evaluation of electron micrographs at 3.5 Å resolution. *Ultramicroscopy* **19,** 147–178.

Herman, G. T., Marabini, R., Carazo, J. M., Garduno, E., Lewitt, R. M., and Matej, S. (2000) Image processing approaches to biological three-dimensional electron microscopy. *Int. J. Imaging Syst. Technol.* **11,** 12–29.

Hoenger, A., and Aebi, U. (1996) 3-D reconstructions from ice-embedded and negatively stained biomacromolecular assemblies: A critical comparison. *J. Struct. Biol.* **117,** 99–116.

Lepault, J. (1985) Cryo-electron microscopy of helical particles TMV and T4 polyheads. *J. Microsc.* **140** (Pt. 1), 73–80.

Marabini, R., Herman, G. T., and Carazo, J. M. (1998) 3D reconstruction in electron microscopy using ART with smooth spherically symmetric volume elements (blobs). *Ultramicroscopy* **72,** 53–65.

Parker, M. L., Christensen, A. C., Boosman, A., Stockard, J., Young, E. T., and Doermann, A. H. (1984) Nucleotide sequence of bacteriophage T4 gene 23 and the amino acid sequence of its product. *J. Mol. Biol.* **180,** 399–416.

Saxton, W. O., and Baumeister, W. (1982) The correlation averaging of a regularly arranged bacterial cell envelope protein. *J. Microsc.* **127,** 127–138.

Saxton, W. O., and Baumeister, W. (1984) Three-dimensional reconstruction of imperfect two-dimensional crystals. *Ultramicroscopy* **13,** 57–70.

Schmid, M. F., Dargahi, R., and Tam, M. W. (1993) SPECTRA—A system for processing electron images of crystals. *Ultramicroscopy* **48,** 251–264.

Steven, A. C., Couture, E., Aebi, U., and Showe, M. K. (1976) Structure of T4 polyheads. II. A pathway of polyhead transformations as a model for T4 capsid maturation. *J. Mol. Biol.* **106,** 187–221.

Walz, T., Tittmann, P., Fuchs, K. H., Müller, D. J., Smith, B. L., Agre, P., Gross, H., and Engel, A. (1996) Surface topographies at subnanometer resolution reveal asymmetry and sidedness of aquaporin-1. *J. Mol. Biol.* **264,** 907–918.

West, J., Fitzpatrick, J. M., Wang, M. Y., Dawant, B. M., Maurer C. R., Kessler, R, M., and Maciunas, R. J. (1999) Retrospective intermodality registration techniques for images of the head: Surface-based versus volume-based. *IEEE Trans. Med. Imag.* **18**(2), 144–150.